ACS OMEGA

Article

Cite This: ACS Omega 2019, 4, 3832−3838

http://pubs.acs.org/journal/acsodf

Effect of Water on the Manifestation of the Reaction Selectivity of Nitrogen-Doped Graphene Nanoclusters toward Oxygen Reduction Reaction

Haruyuki Matsuyama,*[,†,‡] Akira Akaishi,[†,‡] and Jun Nakamura*[,†,‡]

[†]Department of Engineering Science, The University of Electro-Communications (UEC-Tokyo), 1-5-1 Chofugaoka, Chofu, Tokyo 182-8585, Japan

[‡]CREST, Japan Science and Technology Agency, 4-1-8 Honcho, Kawaguchi, Saitama 332-0012, Japan

Supporting Information

ABSTRACT: We investigated the selectivity of N-doped graphene nanoclusters (N-GNCs) toward the oxygen reduction reaction (ORR) using first-principles calculations within the density functional theory. The results show that the maximum electrode potentials (U_{Max}) for the four-electron ($4e^-$) pathway are higher than those for the two-electron ($2e^-$) pathway at almost all of the reaction sites. Thus, the N-GNCs exhibit high selectivity for the $4e^-$ pathway, that is, the $4e^-$ reduction proceeds preferentially over the $2e^-$ reduction. Such high selectivity results in high durability of the catalyst because H_2O_2, which corrodes the electrocatalyst, is not generated. For the doping sites near the edge of the cluster, the value of U_{Max} greatly depends on the reaction sites. However, for the doping sites around the center of the cluster, the reaction-site dependence is hardly observed. The GNC with a nitrogen atom around the center of the cluster exhibits higher ORR catalytic capability compared with the GNC with a nitrogen atom in the vicinity of the edge. The results also reveal that the water molecule generated by the ORR enhances the selectivity toward the $4e^-$ pathway because the reaction intermediates are significantly stabilized by water.

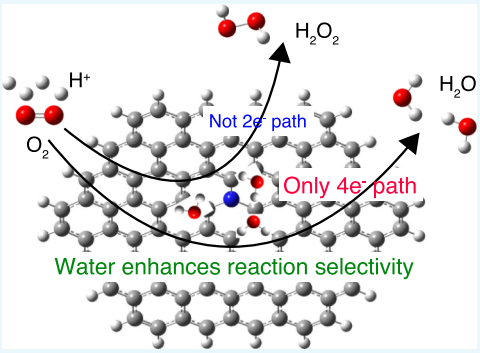

INTRODUCTION

Fuel cells have recently attracted much attention as eco-friendly energy systems. In a fuel cell, energy is obtained through an electrochemical reaction of hydrogen fuel with oxygen. The main problem impeding the widespread implementation of fuel cells is that the oxygen reduction reaction (ORR) at the cathode is less efficient than the hydrogen oxidation reaction at the anode. Currently, platinum-based materials are being commonly used as effective catalysts for the ORR. However, platinum-based materials have many problems, including high cost and low durability. Therefore, a platinum-free catalyst with the high ORR activity is required. N-doped graphene is expected to be one such electrocatalyst materials. Recently, N-doped graphene has been experimentally confirmed to exhibit high ORR activity.[1−9] Although various aspects of the ORR mechanism have been proposed, such as the type of C−N bonding, the presence of local active sites, and the effects of edges, little consensus exists about the mechanism that N-doped graphene follows to promote the ORR at the atomic scale. Many researchers have suggested on the basis of experimentation that the N-doped graphene containing pyridinic-N exhibits high ORR activity.[2−6] Wu et al. have reported that N-doped graphene can be synthesized from g-C_3N_4 and have suggested that the pyridinic-N tends to be the most active N functional group to facilitate ORR at low overpotential.[4] Zeng has suggested that highly graphitized carbon with high contents of pyridinic-N and graphitic-N at the edge exhibits higher ORR activity.[6] With respect to the active site, a C atom adjacent to a pyridinic-N can potentially function as an active site where an O_2 molecule can be adsorbed in the initial step of the ORR.[5] In contrast, Geng et al. have claimed that graphitic-N species appear to play a predominant role in determining the ORR activity.[9] Our previous calculations[10] have also suggested that the graphitic-N is capable of providing reaction sites for ORR.

To improve the electrocatalytic performances of N-doped graphene, increasing the number of active sites is critical. In this respect, small graphene surrounded by edges, that is, graphene nanoclusters (GNCs), have attracted much attention. High-symmetry GNCs with various shapes and sizes have been fabricated experimentally.[11−17] Because N atoms get preferentially doped at edges that exhibit high chemical reactivity,[18−21] numerous theoretical studies on the ORR activity at edges and defects of N-doped graphene have been reported.[22−28] The C atoms near the N atoms at the edge have been identified as the ORR active sites.[24−28] For example, Saidi has suggested that

Received: January 2, 2019
Accepted: February 7, 2019
Published: February 21, 2019

DOI: 10.1021/acsomega.9b00015
ACS Omega 2019, 4, 3832−3838

both pyridinic- and graphitic-N are dominant active sites at the edge of the N-doped nanocarbons.[28] Furthermore, the electronic structure near the doped N atom has been suggested to drastically change depending on the distance of the N atom from the edge.[20,21,29] However, little attention has been devoted to the dependence of the ORR activity on doping and active sites in the vicinity of the edge.

In general, the ORR mainly proceeds via two pathways: a two-electron ($2e^-$) pathway wherein O_2 molecules are reduced to hydrogen peroxides (H_2O_2) and a direct four-electron ($4e^-$) pathway wherein the final product of the reaction is water.[4,26,30−36] H_2O_2 generated by the $2e^-$ reaction might corrode a carbon-based electrocatalyst causing poor device durability. Thus, the $4e^-$ pathway is more desirable than the $2e^-$ pathway; hence, selectivity for the $4e^-$ pathway is required for the carbon-based catalyst. The discussion of reaction selectivity has thus far focused on metal-based catalysts. The reaction selectivity on metal surfaces strongly depends on the metals and their surface orientations,[37] and it is dominated by the stability of reaction intermediates adsorbed on the metal surface. However, the onset of the reaction selectivity is not fully understood. The stability of reaction intermediates has been suggested to be affected by environmental water. For example, ORR intermediates have been demonstrated to be stabilized by the environmental water on the surface of a Pt catalyst.[38,39] For N-doped graphene, the stability of adsorbed O_2 molecules is strongly affected by environmental water.[36] Further, it has also been reported that the ORR activity is strongly influenced by water molecules generated by the ORR itself.[40] However, the effects of water on the reaction selectivity have not been clarified.

To comprehensively evaluate the catalytic activity for ORR, it is necessary to understand the reaction kinetics as well as thermodynamics. However, in the first place, the thermodynamic properties of ORR should be revealed before the reaction kinetics because a potential of the ORR activity is governed by the thermodynamical stability for each reaction process. In the present work, we use first-principles calculations based on the density functional theory (DFT) to investigate the effects of doping and reaction sites on the ORR activity of the N-doped graphene nanoclusters (N-GNCs) in view of the thermodynamical selectivity for the reaction pathway. We focus on the effect of the water molecule generated by the reaction on the ORR activity. We show that high selectivity toward the $4e^-$ pathway is attained for GNCs with N atoms located at the inner doping sites of the cluster rather than at the edge sites. We also suggest that the water molecule plays a critical role in the manifestation of the reaction selectivity.

Figure 1 shows the model of the GNC, in which a C atom is substituted by a N atom. We adopted the hexagonal N-GNCs with zigzag edges which have been fabricated experimentally.[17] The doping and the reaction sites are denoted by numbers and letters, respectively (see Figure 1). We assumed that the reaction sites are C atoms adjacent to the N atom, onto which the reaction intermediates (O, OH, and OOH) for the ORR are adsorbed (see Figure 2). We define model "x−y" as a model for doping site "x" and reaction site "y".

RESULTS AND DISCUSSION

Figure 3 shows the relative formation energies of the N-GNCs. The N atom preferentially located at the edge, at sites 1 and 1′, rather than at the inner site of the cluster, which agrees well with previous results.[19−21] The edge-localized states[41] on

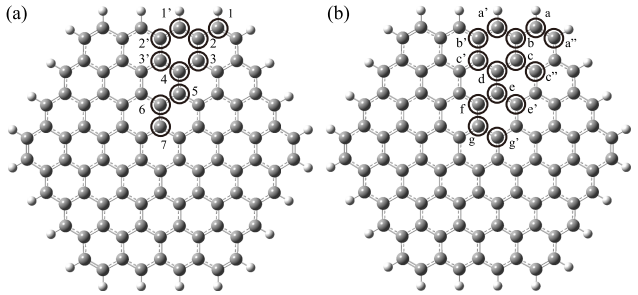

Figure 1. Model of the N-GNC ($C_{95}H_{24}N$). The white and gray balls indicate H and C atoms, respectively. (a) Numbers 1−7 and (b) symbols a−g indicate doping sites and reaction sites, respectively.

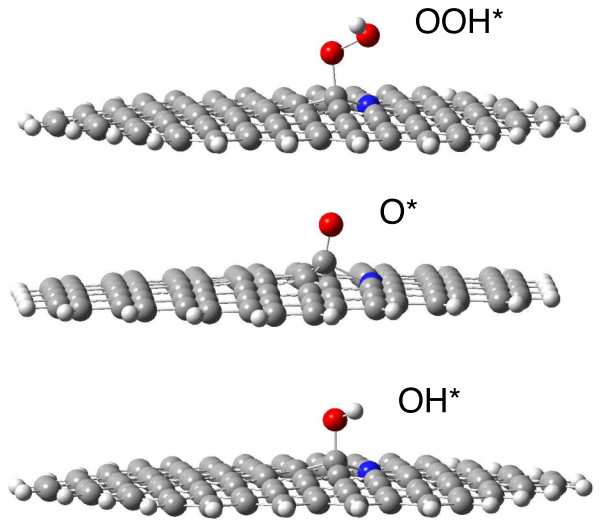

Figure 2. Model of the ORR intermediates on the N-GNC. The white, gray, blue, and red balls indicate H, C, N, and O atoms, respectively.

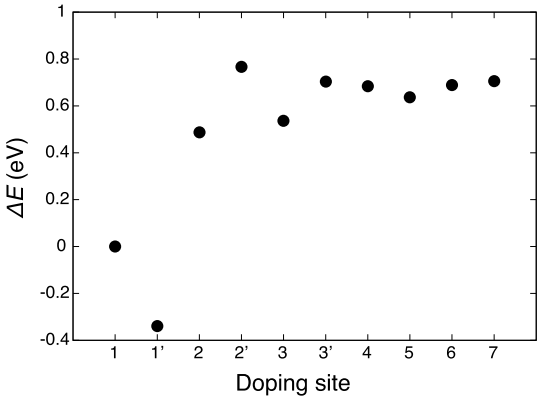

Figure 3. Relative formation energy of the H-terminated N-GNC for each doping site. The total energy for site 1 is set to be zero.

zigzag edges strongly affect the doping stability as follows:[21] for N-doping on the zigzag graphene nanoribbon (GNR), the formation energy increased as a function of the distance of N from the edge and two independent curves arose for odd- and even-numbered sites. Because the wave function of the edge state has amplitude only at odd-numbered sites, only the N $2p_z$ orbital at odd-numbered sites can resonate with the edge state. As a result, the eigenvalue of the edge state for the odd-numbered-site doping became lower than that for the even-

DOI: 10.1021/acsomega.9b00015
ACS Omega 2019, 4, 3832−3838

numbered-site doping. For GNCs, the edge states apparently emerged at the edges of GNCs larger than $C_{96}H_{24}$.[29] For our model ($C_{96}H_{24}$), the number of edge atoms was too small to clearly produce the localized state at the edge. Therefore, such an odd−even trend in the formation energy was not observed distinctly in our cluster model.

As evident in Figure 3, the N atom was preferentially located at site 1′ rather than at site 1. N atoms have been reported to preferentially locate at the zigzag edges rather than at armchair edges.[20] Site 1′ was deemed to be a pure zigzag edge, whereas site 1 was regarded as either the side or the corner of the cluster—namely, zigzag as well as armchair edges. Therefore, site 1′ became more stable than site 1. In this study, each N atom located at site 1 or 1′ was terminated by a H atom, despite the apparent improbability of such an arrangement. The N atom of a pyridine molecule is rarely accompanied by a H atom because the N atom of pyridine has a stable lone pair of electrons. However, the N atom at the zigzag edge preferred to be hydrogenated, maintaining the planar C−N−C structure. The formation of a stable N−H bond at the zigzag edge of GNR corroborated the charge-transfer model:[21] if the extra electron transfers to the edge state, one of the electrons of N contributes to the formation of the covalent bonding between N and H, and then the π-conjugated network near the edge is preserved even with N-doping. The stability of the N−H bond for N-GNC cannot be discussed the same way as that of the N−H bond for GNR because the edge state hardly emerged in our ($C_{96}H_{24}$) model. In fact, at doping site 1, the pyridinic-N was more stable than N terminated by a H atom. The quantitative stability of the N−H bond was shown in the Supporting Information.

In the present work, the value of U_{Max} with respect to a standard hydrogen electrode (SHE) and the reaction selectivity were evaluated using free-energy diagrams. Figure 4 shows the free-energy diagrams for model 7-f as an example. In these diagrams, the free energies of the ORR intermediates are plotted from O_2 toward the final product of the ORR at zero-cell potential (U = 0 V), the equilibrium potential (U_{eq}), and the maximum potential (U_{Max}), wherein all reaction steps are exothermic. At U = 0 V, the diagram for the 4e$^-$ pathway becomes downhill: all of the reactions spontaneously proceed toward the generation of H_2O. The U_{Max} calculated for the 4e$^-$ pathway is 0.68 V. By contrast, for the 2e$^-$ pathway, the diagram becomes uphill from the OOH adsorption to the H_2O_2 generation at U = 0 V, which causes a negative value of U_{Max} (−0.13 V). Thus, the ORR for the 2e$^-$ pathway stops at the OOH adsorption step, and H_2O_2 generation is thereby suppressed. All of the corresponding reaction diagrams are shown in the Supporting Information.

We evaluated the ORR activity of the N-GNC for each doping site and reaction site by estimating U_{Max} in terms of the output voltage or the durability, that is, the reaction selectivity, of fuel cells. Figure 5 shows the variation of U_{Max} depending on the doping and the reaction sites. The U_{Max} for the 4e$^-$ pathway is higher than that for the 2e$^-$ one for each doping and each reaction site except for the 1-b, pyridinic 1-b, and 2-a models. The highest U_{Max} for the 4e$^-$ pathway for any doping sites is ≈0.7−0.8 V, comparable to that for platinum (U_{Max} = 0.9 V[42]). Although the values of U_{Max} are greatly scattered near the edge, the reaction site variation of U_{Max} is reduced for the doping sites inside the cluster (≥site 3). The average U_{Max} for inner doping sites (≥site 3) of the clusters is 0.76 and 0.01 V for the 4e$^-$ and the 2e$^-$ pathways (see dashed and dotted lines in Figure 5), respectively. Notably, the values of U_{Max} for the 2e$^-$ pathway are approximately negative numbers except for those corresponding to doping at the edge. When U_{Max} becomes negative, the reaction does not occur unless the reverse voltage is applied. Thus, the N-GNCs have high selectivity for the 4e$^-$ pathway, that is, the ORR via the 4e$^-$ pathway proceeds preferentially. However, for the doping sites in the vicinity of the edge (<site 3), the values of U_{Max} depend strongly on the reaction sites. For example, for the model 1-a″, the U_{Max} for the 4e$^-$ pathway becomes a negative value. In this case, the ORR is aborted at the OH adsorption step, and the reaction site then becomes inactive for the ORR. Furthermore,

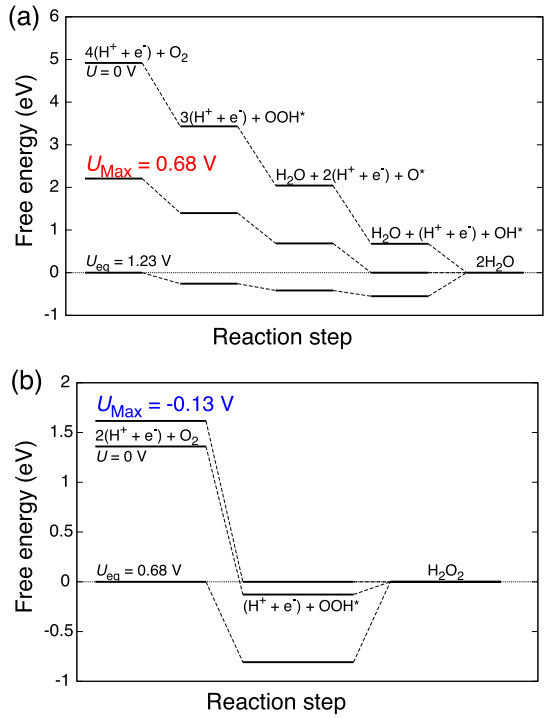

Figure 4. Free-energy diagrams of the model 7-f under acidic conditions (a) for the 4e$^-$ pathway at zero cell potential (U = 0 V), the equilibrium potential (U_{eq} = 1.23 V), and the maximum potential (U_{Max} = +0.68 V) wherein all reaction steps are exothermic and (b) for the 2e$^-$ pathway at U = 0 V, U_{eq} = 0.68 V, and U_{Max} = −0.13 V.

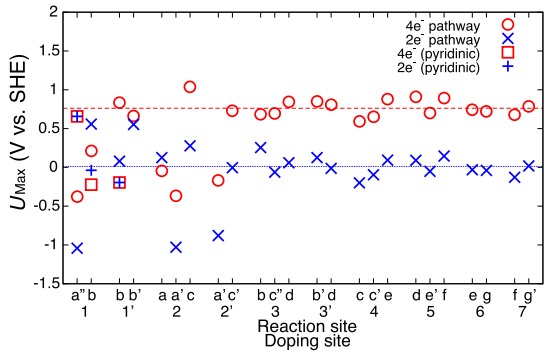

Figure 5. U_{Max} of the N-GNCs for the models. The circles and the crosses show the U_{Max} for the 4e$^-$ and the 2e$^-$ pathways, respectively. The U_{Max} for the pyridinic-N models are indicated by the squares for the 4e$^-$ pathway and by the plus marks for the 2e$^-$ pathway, respectively. The dashed and dotted lines show averaged values of U_{Max} over deeper doping sites (≥site 3) for the 4e$^-$ and the 2e$^-$ pathways, respectively.

DOI: 10.1021/acsomega.9b00015
ACS Omega 2019, 4, 3832−3838

for 1-b and 1′-b, the U_{Max} values for the 2e$^-$ pathway are relatively large and positive as compared with cases for deeper site doping. In such cases, H_2O_2 molecules generated by the 2e$^-$ reaction corrode the electrocatalyst, resulting in poor durability of the fuel cell. Hence, we conclude that high capability for the ORR is more likely to be achieved via the doping of N into a deeper site of the cluster.

The N-GNR has been reported to exhibit high ORR activity in the vicinity of the edge.[27] In our results, the N-GNC also shows a high U_{Max} at the edge sites (1′-b, 2-c, etc.). However, in the vicinity of the edge (<site 3), the values of U_{Max} depend strongly on the reaction sites, and the selectivity for the 4e$^-$ reduction is low. Therefore, the ORR at the edge of the N-GNC is undesirable from the viewpoint of achieving a stable output and a durable fuel cell. Because N atoms thermodynamically prefer to locate near the edges, fabricating N-GNCs containing N atoms inside the clusters in a thermal equilibrium state would be experimentally difficult. However, if the N-GNC containing N atoms inside the cluster can be fabricated using nonequilibrium processes, such as a solution plasma process,[43] the N-GNC becomes an epoch-making catalyst for the ORR.

U_{Max} is determined by the relative free energies of the intermediates, ΔG_{OOH}, ΔG_O, and ΔG_{OH}. For the 4e$^-$ pathway, the state of equilibrium between OH adsorption and H_2O generation dominates the value of U_{Max} for almost all of the models. Figure 6 shows the ΔG values for the models. For

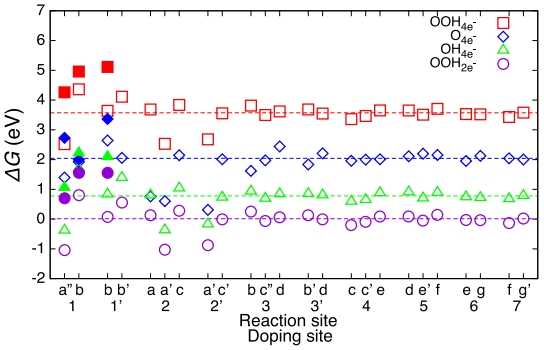

Figure 6. ΔG values of the reaction intermediates for the models. The squares, rhombuses, and triangles represent ΔG_{OOH}, ΔG_O, and ΔG_{OH} values for the 4e$^-$ pathway, respectively. The circles represent ΔG_{OOH} values for the 2e$^-$ pathway. The free energies for pyridinic-N models are indicated by filled marks. The dashed lines show the averaged ΔG values for the reaction intermediates over deeper doping sites (≥site 3).

inner doping sites (≥site 3) of the clusters, the ΔG values are almost the same, regardless of the reaction site. By contrast, for the doping sites in the vicinity of the edge (<site 3), ΔG varies depending on the reaction site, which leads to a substantial dependence of U_{Max} on the reaction site. Furthermore, for the pyridinic-N models, the values of ΔG are higher than those for the graphitic-N models, that is, each intermediate for the pyridinic-N models is relatively unstable. When the reaction site is just at the edge, ΔG_{OH} becomes a negative value for site 1-a″, 2-a′, and 2′-a′. This result means that the reaction is aborted at the step of OH adsorption, and that these reaction sites are then no longer active.

We explicitly investigated the influence of water (ΔG_W) on the adsorption of a water molecule onto reaction intermediates to evaluate the ORR activity because the adsorption energy of reaction intermediates is strongly affected by water. Hydrogen bonding between a reaction intermediate and a water molecule stabilizes the intermediates of the ORR. Water molecules have been reported to affect the stability of the OOH and the OH adsorbed onto the surface of the metal catalyst, whereas the adsorption energy of O has been reported to be hardly affected by water.[38] However, for the N-GNCs, the adsorbed O is stabilized by a water molecule as well as the adsorption of OOH or OH. Figure 7 shows the ΔG_W for all models. The

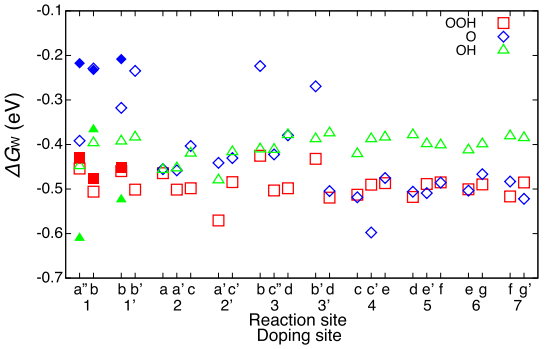

Figure 7. ΔG_W of the reaction intermediates for each doping site and reaction site. The squares, rhombuses, and triangles represent ΔG_W(OOH), ΔG_W(O), and ΔG_W(OH), respectively. The ΔG_W for pyridinic-N models are indicated by the filled marks.

values of ΔG_W(OOH) and ΔG_W(OH) are approximately −0.5 and −0.4 eV, respectively. The value of ΔG_W(OOH) and ΔG_W(OH) are roughly independent of the doping site. However, ΔG_W(O) in the vicinity of the edge varies depending on the doping sites, whereas the values of ΔG_W(O) for inner doping sites (≥site 4) of the clusters are settled. As shown in Figure 8, the maximum electrode potentials without the

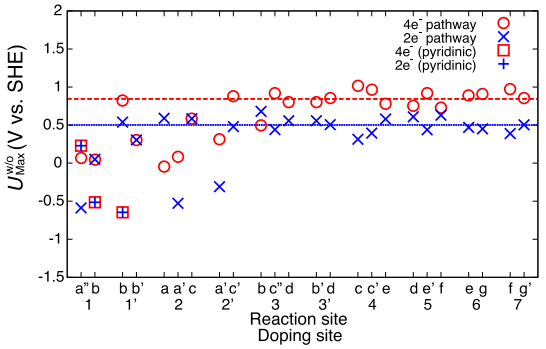

Figure 8. $U_{Max}^{w/o}$ of the N-GNCs for the models; maximum electrode potentials without the adsorption of a water molecule. The circles and the crosses show $U_{Max}^{w/o}$ for the 4e$^-$ and the 2e$^-$ pathways, respectively. The $U_{Max}^{w/o}$ for the pyridinic-N models are indicated by squares and the plus marks for the 4e$^-$ and the 2e$^-$ pathways, respectively. The dashed and dotted lines show the average $U_{Max}^{w/o}$ for the 4e$^-$ and the 2e$^-$ pathways over deeper doping sites (≥site 3), respectively.

adsorption of a water molecule, denoted by the value of $U_{Max}^{w/o}$ for the 4e$^-$ pathway, are approximately the same as U_{Max} (Figure 5). However, the $U_{Max}^{w/o}$ for the 2e$^-$ pathways are substantially greater than the U_{Max}; in addition, the $U_{Max}^{w/o}$ of the 4e$^-$ pathway is still greater than those for the 2e$^-$ pathway except for 2-a and 3-b. Thus, almost all models show selectivity for the 4e$^-$ pathway (such as the ORR with ΔG_W). However, the $U_{Max}^{w/o}$ values of the 2e$^-$ pathway are positive and relatively

DOI: 10.1021/acsomega.9b00015
ACS Omega 2019, 4, 3832−3838

large values ≈0.5 V because the ΔG_{OOH}, which dominates the maximum electrode potential for the 2e$^-$ pathway, increases in the absence of water. As a result, the 2e$^-$ reduction as well as the 4e$^-$ reduction must proceed. Hence, the water plays an important role in the onset of the reaction selectivity. It has been reported that the removal of water molecules at the Pt-catalyst surface enhances the reactivity of oxygen species.[44] Furthermore, for Pt-based catalysts, water molecules have been reported to corrode the catalyst and to substantially decrease the electrocatalytic performance for the ORR.[40] Therefore, to improve the ORR activity of Pt-based catalysts, water molecules should be removed in the reaction field. On the other hand, for the N-GNCs, the water rather improves the reaction selectivity, resulting in high durability of the fuel cell. This durability will be a great advantage of N-GNCs over metal-based catalysts.

CONCLUSIONS

The ORR activity for the hexagonal N-GNCs was investigated. The GNC with a nitrogen atom around the center of the cluster exhibits a high U_{Max} and high selectivity for the 4e$^-$ pathway, that is, it exhibits high durability. For the doping sites near the edge, the value of U_{Max} depends strongly on both the doping and the reaction sites, resulting in low selectivity for the 4e$^-$ pathway. However, for the doping sites inside the cluster, the lack of a significant dependence of U_{Max} on the doping and the reaction sites is confirmed. Furthermore, we clarified that the reaction intermediates are stabilized by the water molecule, resulting in high selectivity for the 4e$^-$ reduction. This behavior contrasts sharply with those of metal-based catalysts, where water molecules corrode and substantially decrease its ORR electrocatalytic performance.[40] We concluded that from the viewpoint of durability under a water environment, the N-GNC with a N atom inside the cluster is a potential electrocatalyst for next-generation fuel cells.

COMPUTATIONAL METHODS

For all DFT calculations, we used the Gaussian 09 code[45] employing the hybrid B3LYP functional[46,47] and the 6-31G (d,p) basis set in this package. Structural optimization with respect to ionic positions was performed until each component of the interatomic force was <0.0003 Ha/bohr. The ORR for the 4e$^-$ pathway is ideally facilitated just below the equilibrium potential (1.23 V). For the 4e$^-$ pathway, O_2 is reduced to H_2O through the intermediates OOH, O, and OH. We considered the following associative mechanism

$$\begin{aligned} &4(H^+ + e^-) + O_2 \rightarrow 3(H^+ + e^-) + OOH^* \\ &3(H^+ + e^-) + OOH^* \rightarrow H_2O + 2(H^+ + e^-) + O^* \\ &H_2O + 2(H^+ + e^-) + O^* \rightarrow H_2O + (H^+ + e^-) + OH^* \\ &H_2O + (H^+ + e^-) + OH^* \rightarrow 2H_2O \end{aligned} \quad (1)$$

where "*" denotes that the ORR intermediates are adsorbed onto the surface of the catalyst. The ORR for the 2e$^-$ pathway is ideally facilitated just below the equilibrium potential (0.68 V). For the 2e$^-$ pathway, O_2 molecules are reduced to H_2O_2 through the intermediate of OOH. An associative mechanism was also considered for the 2e$^-$ pathway

$$\begin{aligned} &2(H^+ + e^-) + O_2 \rightarrow (H^+ + e^-) + OOH^* \\ &(H^+ + e^-) + OOH^* \rightarrow H_2O_2 \end{aligned} \quad (2)$$

For the 2e$^-$ pathway, the process of H_2O_2 reduction is excluded because a H_2O_2 molecule is desorbed from the N-GNC without an activation barrier. The electrocatalytic activities for the 4e$^-$ and 2e$^-$ reductions are dominated by the stability of adsorption of the intermediates OOH, O, and OH.

The ORR electrocatalytic activities were evaluated on the basis of the computational hydrogen electrode model proposed by Nørskov.[48] The chemical potential for $(H^+ + e^-)$ is equivalent to that of $1/2H_2$ in the gas phase with the SHE. We considered the free-energy difference (ΔG) of the ORR processes with a pressure of 1 bar, pH = 0, and T = 298 K.

The ΔG was constructed as follows

$$\Delta G = \Delta G_0 + \Delta G_U + \Delta G_{pH} + \Delta G_W + \Delta G_{field} \quad (3)$$

where ΔG_0 is the Gibbs free energy, ΔG_U corresponds to the electrode potential, ΔG_{pH} represents the effect of the solvent, ΔG_W is the stabilization energy by water, and ΔG_{field} is the effect of the local electric field at the electrode. The ΔG_0 was calculated considering the following terms

$$\Delta G_0 = \Delta E + \Delta ZPE - T\Delta S \quad (4)$$

where ΔE is the energy difference between reaction intermediates and final products and ΔZPE and $T\Delta S$ means the zero-point energy and the entropy, respectively. ΔZPE and $T\Delta S$ were computed by the vibrational frequency calculation. Here, ΔE values were calculated for the 4e$^-$ pathway

$$\begin{aligned} \Delta E_{O_2} &= 1.23\ \text{V} \times 4\text{e} = 4.92\ \text{eV} \\ \Delta E_{OOH} &= E(OOH^*) - E(^*) + \frac{3}{2}E(H_2) - 2E(H_2O) \\ \Delta E_O &= E(O^*) - E(^*) + E(H_2) - E(H_2O) \\ \Delta E_{OH} &= E(OH^*) - E(^*) + \frac{1}{2}E(H_2) - E(H_2O) \end{aligned} \quad (5)$$

and for the 2e$^-$ pathway

$$\begin{aligned} \Delta E_{O_2} &= 0.68\ \text{V} \times 2\text{e} = 1.36\ \text{eV} \\ \Delta E_{OOH} &= E(OOH^*) - E(^*) + \frac{3}{2}E(H_2) - 2E(H_2O) \\ &\quad - 3.56\ \text{eV} \end{aligned} \quad (6)$$

We assumed that ΔG_W is the stabilization energy by a water molecule. Here, we optimized the hydrogen-bonding configuration between each reaction intermediate and a water molecule for all models. Typical values of ΔG_W are −0.49 (OOH), −0.52 (O), and −0.39 eV (OH) for the model 7-g′, which agree well with the results for the effect of several water layers, −0.49 (OOH), −0.53 (O), and −0.42 eV (OH),[36] respectively. We set ΔG_{pH} = 0, that is, the acidic condition (pH = 0). We ignored the term ΔG_{field} because the absolute value of ΔG_{field} was estimated to be very small (≈10^{-2} eV).[49] By changing ΔG_U, we estimated the maximum electrode potential (U_{Max}) wherein all reaction steps are exothermic for the 4e$^-$ and the 2e$^-$ pathways.

DOI: 10.1021/acsomega.9b00015
ACS Omega 2019, 4, 3832−3838

■ ASSOCIATED CONTENT

Supporting Information

The Supporting Information is available free of charge on the ACS Publications website at DOI: 10.1021/acsomega.9b00015.

Stability of H-terminated edge N; reaction free energies without ΔG_W; and free-energy diagrams (PDF)

■ AUTHOR INFORMATION

Corresponding Authors

*E-mail: matsuyama@natori.ee.uec.ac.jp. Phone: +81 (0)42 4435156. Fax: +81 (0)42 4435156 (H.M.).
*E-mail: junj@ee.uec.ac.jp (J.N.).

ORCID

Haruyuki Matsuyama: 0000-0002-6241-129X
Akira Akaishi: 0000-0001-8013-2131
Jun Nakamura: 0000-0001-8909-4645

Notes

The authors declare no competing financial interest.

■ ACKNOWLEDGMENTS

This work was supported by CREST, Japan Science and Technology Agency.

■ REFERENCES

(1) Panomsuwan, G.; Saito, N.; Ishizaki, T. Electrocatalytic oxygen reduction on nitrogen-doped carbon nanoparticles derived from cyano-aromatic molecules via a solution plasma approach. *Carbon* **2016**, *98*, 411−420.

(2) Sun, J.; Wang, L.; Song, R.; Yanga, S. Enhancing pyridinic nitrogen level in graphene to promote electrocatalytic activity for oxygen reduction reaction. *Nanotechnology* **2016**, *27*, 055404.

(3) Lee, K. R.; Lee, K. U.; Lee, J. W.; Ahn, B. T.; Woo, S. I. Electrochemical oxygen reduction on nitrogen doped graphene sheets in acid media. *Electrochem. Commun.* **2010**, *12*, 1052−1055.

(4) Wu, J.; Ma, L.; Yadav, R. M.; Yang, Y.; Zhang, X.; Vajtai, R.; Lou, J.; Ajayan, P. M. Nitrogen-Doped Graphene with Pyridinic Dominance as a Highly Active and Stable Electrocatalyst for Oxygen Reduction. *ACS Appl. Mater. Interfaces* **2015**, *7*, 14763−14769.

(5) Guo, D.; Shibuya, R.; Akiba, C.; Saji, S.; Kondo, T.; Nakamura, J. Active sites of nitrogen-doped carbon materials for oxygen reduction reaction clarified using model catalysts. *Science* **2016**, *351*, 361−365.

(6) Zeng, D.; Yu, X.; Zhan, Y.; Cao, L.; Wu, X.; Zhang, B.; Huang, J.; Lin, Z.; Xie, F.; Zhang, W.; et al. Insight into the nitrogen-doped carbon as oxygen reduction reaction catalyst: The choice of carbon/nitrogen source and active sites. *Int. J. Hydrogen Energy* **2016**, *41*, 8563−8575.

(7) Yang, S.-Y.; Chang, K.-H.; Huang, Y.-L.; Lee, Y.-F.; Tien, H.-W.; Li, S.-M.; Lee, Y.-H.; Liu, C.-H.; Ma, C.-C. M.; Hu, C.-C. A powerful approach to fabricate nitrogen-doped graphene sheets with high specific surface area. *Electrochem. Commun.* **2012**, *14*, 39−42.

(8) Soin, N.; Roy, S. S.; Sharma, S.; Thundat, T.; McLaughlin, J. A. Electrochemical and oxygen reduction properties of pristine and nitrogen-doped few layered graphene nanoflakes (FLGs). *J. Solid State Electrochem.* **2013**, *17*, 2139−2149.

(9) Geng, D.; Chen, Y.; Chen, Y.; Li, Y.; Li, R.; Sun, X.; Ye, S.; Knights, S. High oxygen-reduction activity and durability of nitrogen-doped graphene. *Energy Environ. Sci.* **2011**, *4*, 760−764.

(10) Matsuyama, H.; Akaishi, A.; Nakamura, J. Reaction Selectivity for Oxygen Reduction of N-doped Graphene Nanoclusters. *ECS Trans.* **2017**, *80*, 685−690.

(11) Ci, L.; Song, L.; Jariwala, D.; ElÃas, A. L.; Gao, W.; Terrones, M.; Ajayan, P. M. Graphene Shape Control by Multistage Cutting and Transfer. *Adv. Mater.* **2009**, *21*, 4487−4491.

(12) Robertson, A. W.; Warner, J. H. Hexagonal Single Crystal Domains of Few-Layer Graphene on Copper Foils. *Nano Lett.* **2011**, *11*, 1182−1189.

(13) Lu, J.; Yeo, P. S. E.; Gan, C. K.; Wu, P.; Loh, K. P. Transforming C60 molecules into graphene quantum dots. *Nat. Nanotechnol.* **2011**, *6*, 247−252.

(14) Geng, D.; Wu, B.; Guo, Y.; Huang, L.; Xue, Y.; Chen, J.; Yu, G.; Jiang, L.; Hu, W.; Liu, Y. Uniform hexagonal graphene flakes and films grown on liquid copper surface. *Proc. Natl. Acad. Sci. U.S.A.* **2012**, *109*, 7992−7996.

(15) Han, G. H.; Rodríguez-Manzo, J. A.; Lee, C.-W.; Kybert, N. J.; Lerner, M. B.; Qi, Z. J.; Dattoli, E. N.; Rappe, A. M.; Drndic, M.; Johnson, A. T. C. Continuous Growth of Hexagonal Graphene and Boron Nitride In-Plane Heterostructures by Atmospheric Pressure Chemical Vapor Deposition. *ACS Nano* **2013**, *7*, 10129−10138.

(16) Luo, Z.; Kim, S.; Kawamoto, N.; Rappe, A. M.; Johnson, A. T. C. Growth Mechanism of Hexagonal-Shape Graphene Flakes with Zigzag Edges. *ACS Nano* **2011**, *5*, 9154−9160.

(17) Wei, D.; Peng, L.; Li, M.; Mao, H.; Niu, T.; Han, C.; Chen, W.; Wee, A. T. S. Low Temperature Critical Growth of High Quality Nitrogen Doped Graphene on Dielectrics by Plasma-Enhanced Chemical Vapor Deposition. *ACS Nano* **2015**, *9*, 164−171.

(18) Wang, X.; Li, X.; Zhang, L.; Yoon, Y.; Weber, P. K.; Wang, H.; Guo, J.; Dai, H. N-Doping of Graphene Through Electrothermal Reactions with Ammonia. *Science* **2009**, *324*, 768−771.

(19) Huang, S.-F.; Terakura, K.; Ozaki, T.; Ikeda, T.; Boero, M.; Oshima, M.; ichi Ozaki, J.; Miyata, S. First-principles calculation of the electronic properties of graphene clusters doped with nitrogen and boron: Analysis of catalytic activity for the oxygen reduction reaction. *Phys. Rev. B: Condens. Matter Mater. Phys.* **2009**, *80*, 235410.

(20) Jiang, J.; Turnbull, J.; Lu, W.; Boguslawski, P.; Bernholc, J. Theory of nitrogen doping of carbon nanoribbons: Edge effects. *J. Chem. Phys.* **2012**, *136*, 014702.

(21) Uchida, Y.; Gomi, S.-i.; Matsuyama, H.; Akaishi, A.; Nakamura, J. Mechanism of stabilization and magnetization of impurity-doped zigzag graphene nanoribbons. *J. Appl. Phys.* **2016**, *120*, 214301.

(22) Ni, S.; Li, Z.; Yang, J. Oxygen molecule dissociation on carbon nanostructures with different types of nitrogen doping. *Nanoscale* **2012**, *4*, 1184−1189.

(23) Chai, G.-L.; Hou, Z.; Shu, D.-J.; Ikeda, T.; Terakura, K. Active Sites and Mechanisms for Oxygen Reduction Reaction on Nitrogen-Doped Carbon Alloy Catalysts: Stone-Wales Defect and Curvature Effect. *J. Am. Chem. Soc.* **2014**, *136*, 13629−13640.

(24) Ikeda, T.; Boero, M.; Huang, S.-F.; Terakura, K.; Oshima, M.; Ozaki, J.-i. Carbon Alloy Catalysts: Active Sites for Oxygen Reduction Reaction. *J. Phys. Chem. C* **2008**, *112*, 14706−14709.

(25) Bao, X.; Nie, X.; von Deak, D.; Biddinger, E. J.; Luo, W.; Asthagiri, A.; Ozkan, U. S.; Hadad, C. M. A First-Principles Study of the Role of Quaternary-N Doping on the Oxygen Reduction Reaction Activity and Selectivity of Graphene Edge Sites. *Top. Catal.* **2013**, *56*, 1623−1633.

(26) Ikeda, T.; Hou, Z.; Chai, G.-L.; Terakura, K. Possible Oxygen Reduction Reactions for Graphene Edges from First Principles. *J. Phys. Chem. C* **2014**, *118*, 17616−17625.

(27) Li, M.; Zhang, L.; Xu, Q.; Niu, J.; Xia, Z. N-doped graphene as catalysts for oxygen reduction and oxygen evolution reactions: Theoretical considerations. *J. Catal.* **2014**, *314*, 66−72.

(28) Saidi, W. A. Oxygen Reduction Electrocatalysis Using N-Doped Graphene Quantum-Dots. *J. Phys. Chem. Lett.* **2013**, *4*, 4160−4165.

(29) Akaishi, A.; Ushirozako, M.; Matsuyama, H.; Nakamura, J. Structural stability and aromaticity of pristine and doped graphene nanoflakes. *Jpn. J. Appl. Phys.* **2017**, *57*, 0102BA.

(30) Wu, J.; Zhang, D.; Wang, Y.; Hou, B. Electrocatalytic activity of nitrogen-doped graphene synthesized via a one-pot hydrothermal process towards oxygen reduction reaction. *J. Power Sources* **2013**, *227*, 185−190.

(31) Vikkisk, M.; Kruusenberg, I.; Joost, U.; Shulga, E.; Kink, I.; Tammeveski, K. Electrocatalytic oxygen reduction on nitrogen-doped graphene in alkaline media. *Appl. Catal., B* **2014**, *147*, 369−376.

DOI: 10.1021/acsomega.9b00015
ACS Omega 2019, 4, 3832−3838

(32) Shinde, D. B.; Vishal, V. M.; Kurungot, S.; Pillai, V. K. Electrochemical preparation of nitrogen-doped graphene quantum dots and their size-dependent electrocatalytic activity for oxygen reduction. *Bull. Mater. Sci.* **2015**, *38*, 435−442.
(33) Ma, R.; Ren, X.; Xia, B. Y.; Zhou, Y.; Sun, C.; Liu, Q.; Liu, J.; Wang, J. Novel synthesis of N-doped graphene as an efficient electrocatalyst towards oxygen reduction. *Nano Res.* **2016**, *9*, 808−819.
(34) Niu, W.-J.; Zhu, R.-H.; Yan-Hua; Zeng, H.-B.; Cosnier, S.; Zhang, X.-J.; Shan, D. One-pot synthesis of nitrogen-rich carbon dots decorated graphene oxide as metal-free electrocatalyst for oxygen reduction reaction. *Carbon* **2016**, *109*, 402−410.
(35) Zhang, L.; Xia, Z. Mechanisms of Oxygen Reduction Reaction on Nitrogen-Doped Graphene for Fuel Cells. *J. Phys. Chem. C* **2011**, *115*, 11170−11176.
(36) Yu, L.; Pan, X.; Cao, X.; Hu, P.; Bao, X. Oxygen reduction reaction mechanism on nitrogen-doped graphene: A density functional theory study. *J. Catal.* **2011**, *282*, 183−190.
(37) Viswanathan, V.; Hansen, H. A.; Rossmeisl, J.; Nørskov, J. K. Unifying the 2e- and 4e- Reduction of Oxygen on Metal Surfaces. *J. Phys. Chem. Lett.* **2012**, *3*, 2948−2951.
(38) Rossmeisl, J.; Logadottir, A.; Nørskov, J. K. Electrolysis of water on (oxidized) metal surfaces. *Chem. Phys.* **2005**, *319*, 178−184.
(39) Liu, S.; White, M. G.; Liu, P. Mechanism of Oxygen Reduction Reaction on Pt(111) in Alkaline Solution: Importance of Chemisorbed Water on Surface. *J. Phys. Chem. C* **2016**, *120*, 15288−15298.
(40) Cui, Y.-T.; Harada, Y.; Niwa, H.; Hatanaka, T.; Nakamura, N.; Ando, M.; Yoshida, T.; Ishii, K.; Matsumura, D.; Oji, H.; et al. Wetting Induced Oxidation of Pt-based Nano Catalysts Revealed by In Situ High Energy Resolution X-ray Absorption Spectroscopy. *Sci. Rep.* **2017**, *7*, 1482.
(41) Nakada, K.; Fujita, M.; Dresselhaus, G.; Dresselhaus, M. S. Edge state in graphene ribbons: Nanometer size effect and edge shape dependence. *Phys. Rev. B: Condens. Matter Mater. Phys.* **1996**, *54*, 17954−17961.
(42) Tripković, V.; Skúlason, E.; Siahrostami, S.; Nørskov, J. K.; Rossmeisl, J. The oxygen reduction reaction mechanism on Pt(111) from density functional theory calculations. *Electrochim. Acta* **2010**, *55*, 7975−7981.
(43) Saito, N.; Bratescu, M. A.; Hashimi, K. Solution plasma: A new reaction field for nanomaterials synthesis. *Jpn. J. Appl. Phys.* **2017**, *57*, 0102A4.
(44) Casalongue, H. S.; Kaya, S.; Viswanathan, V.; Miller, D. J.; Friebel, D.; Hansen, H. A.; Nørskov, J. K.; Nilsson, A.; Ogasawara, H. Direct observation of the oxygenated species during oxygen reduction on a platinum fuel cell cathode. *Nat. Commun.* **2013**, *4*, 2817.
(45) Frisch, M. J.; Trucks, G. W.; Schlegel, H. B.; Scuseria, G. E.; Robb, M. A.; Cheeseman, J. R.; Scalmani, G.; Barone, V.; Mennucci, B.; et al. *Gaussian 09*, Revision D.01.; Gaussian Inc.: Wallingford, Connecticut, 2009.
(46) Lee, C.; Yang, W.; Parr, R. G. Development of the Colle-Salvetti correlation-energy formula into a functional of the electron density. *Phys. Rev. B: Condens. Matter Mater. Phys.* **1988**, *37*, 785−789.
(47) Becke, A. D. Density-functional thermochemistry. III. The role of exact exchange. *J. Phys. Chem. B* **1993**, *98*, 5648−5652.
(48) Nørskov, J. K.; Rossmeisl, J.; Logadottir, A.; Lindqvist, L.; Kitchin, J. R.; Bligaard, T.; Jónsson, H. Origin of the Overpotential for Oxygen Reduction at a Fuel-Cell Cathode. *J. Phys. Chem. B* **2004**, *108*, 17886−17892.
(49) Karlberg, G. S.; Rossmeisl, J.; Nørskov, J. K. Estimations of electric field effects on the oxygen reduction reaction based on the density functional theory. *Phys. Chem. Chem. Phys.* **2007**, *9*, 5158−5161.

DOI: 10.1021/acsomega.9b00015
ACS Omega 2019, 4, 3832−3838